JOURNAL OF MATERIALS SCIENCE 28 (1993) 6222–6232

Structural evolution in ZrO_2–Al_2O_3 gels during sintering

WENBANG ZHANG, E. E. LACHOWSKI, F. P. GLASSER
Department of Chemistry, University of Aberdeen, Aberdeen, Meston Walk, AB9 2UE, UK

The crystallization sequence and phase transformation of inorganic ZrO_2–Al_2O_3 gels during heating has been investigated. The effects of incorporating CaO, MgO and Al_2O_3 into gels are reported. The microstructural evolution and crystallization of the gels during firing were observed by TEM, and the gradual disappearance of homogeneity in the gel was found to be related to thermal processing conditions.

1. Introduction

ZrO_2–Al_2O_3 ceramic composites are interesting materials because of their high strength and toughness and good stability in humid atmospheres [1–4]. Development of alumina as a second phase, influences the properties of zirconia ceramics, especially their phase-transformation characteristics [5–7]. Sol–gel processing offers the possibility of achieving ultra-homogeneous mixing in a multicomponent system on a molecular scale, or nearly so, to achieve densification at relatively low temperatures and, by controlling ZrO_2 crystalline size, influence its phase-transformation sequence.

An extensive literature exists on modelling gelation processes, leading to prediction of the kinetics of growth and of the fractal structures of the resulting clusters [8–10], but the structural evolution of the gel precursor and its conversion to a sintered ceramic has not been explored in such detail, despite its obvious importance to the development of ceramic properties.

Sintering is the final stage of transforming a gel to a ceramic. The removal of residual impurities, such as water and anions, occurs during gel sintering by polycondensation and gradual disappearance of pores in the gel, accompanied by further volume shrinkage leading, under optimum condition, to full densification.

The nature of the first-formed crystalline phase during gel sintering is dependent on many factors: the nature of the precursor, dopant (if any) and heating programme. Because of the mechanism of phase-transformation toughening, it is preferable to obtain zirconia as metastable t-ZrO_2 or c-ZrO_2 and to be able to stabilize partially these polymorphs to ambient. The sequence and rate of ZrO_2 phase transformations is complex, but its solid solutions with a number of oxides, such as Y_2O_3, MgO, CaO, CeO_2, and rare-earths are one important means of controlling its polymorphism [11, 12].

Phase stability is also a function of particle size, because extremely fine particles of ZrO_2 tend to persist as the tetragonal or cubic polymorphs. This stabilization is a consequence of differences of surface free energies between phases [13, 14]. Strain energy and kinetics may also make some contribution to this phase transformation [15, 16], but they can be neglected for a purely sol–gel derived powder because of the absence of a rigid matrix.

A new inorganic sol–gel processing route to ZrO_2–Al_2O_3 composites has been described previously [17]. The mechanism of sol–gel transformation, the gel structure and its thermal decomposition have also been investigated [18, 19]. In the present research, the microstructural evolution of ZrO_2–Al_2O_3-based gels derived from inorganic precursors is related to the nature of precursors and their pyroprocessing.

2. Experimental procedure

2.1. Sample preparation

The main precursors used were zirconia sol, which, upon analysis, was found to correspond to $Zr(OH)_{2.95}(NO_3)_{1.05}$ [20] (Banbury Laboratory, Alcan International Ltd) and $Al_2(OH)_5Cl$ (Albright and Wilson Ltd). The solutions were 3.65 and 6.17 M in zirconium and aluminium, respectively, and are referred to as ZrO_2 and Al_2O_3 sols, respectively.

To initiate reaction, these two sols were mixed in a predetermined ratio with stirring. Once formed, the gel was aged at 20 °C and 100% humidity to prevent water loss by evaporation. All samples intended for thermal treatment and subsequent examination by X-ray diffraction (XRD) and TEM were ramped at 15 °C min^{-1} from room temperature to the selected temperature with a uniform dwell time of 2 h at each isothermal hold.

2.2. X-ray diffraction

X-ray powder diffraction was used to identify phase compositions and to follow phase transformations. A Philips PW1710 diffractometer was used. The specimens were prepared by sprinkling the powder on a glass slide smeared with vaseline. Copper K_α radiation (K_α = 0.154 18 nm) was used; spectra were recorded on a strip chart. All X-ray d-spacings are measured at

0022–2461

ambient temperature. The mean crystallite sizes were determined using the equation [21, 22]

$$L = kW_l/[(B^2 - b^2)]^{1/2} \cos\theta \quad (1)$$

where L, the crystallite size, is related to the differences in half-width of a reflection at diffracting angle θ; B is its width at half maximum intensity and b is the characteristic width for the well-crystallized phase; k is a constant taken as 1, and W_l the wavelength, in this case, 0.154 18 nm. Strain is assumed to make a negligible contribution to line broadening. Two pairs of reflections occur in the range between 18.5° and 36.5° (2θ, CuK_α) for ZrO_2 (t) and ZrO_2 (c) diffractions. They were deconvoluted, assuming both to be symmetrical. The phase ratio between monoclinic (m) and metastable tetragonal (t) or cubic (c) in the coexistence region were calculated by measuring the intensities of the $(1\,1\,1)_m$, $(\bar{1}\,1\,1)_m$ and $(1\,1\,1)_t$ or $(1\,1\,1)_c$ reflections and applying the following equation [23, 24]

$$f_m = [I_m(1\,1\,1) + I_m(\bar{1}\,1\,1)]/[I_m(1\,1\,1) + I_m(\bar{1}\,1\,1) + I_{t/c}(1\,1\,1)] \quad (2)$$

where f_m is the weight fraction of monoclinic phase, and $I_m(1\,1\,1)$, $I_m(\bar{1}\,1\,1)$, $I_t(1\,1\,1)$ and $I_c(1\,1\,1)$ denote the intensity of the $(1\,1\,1)_m$, $(\bar{1}\,1\,1)_m$, $(1\,1\,1)_t$ and $(1\,1\,1)_c$ diffraction peaks, respectively. Evans *et al.* have shown that errors of up to 20% may occur when using Equation 2 to calculate the ratio of monoclinic to tetragonal zirconia phases [24]. To reduce these errors, some researchers have developed other methods [22, 25–27]. In the present work, two calibration curves were applied to obtain the actual ratio of monoclinic and tetragonal/cubic phases present. These curves were obtained from a set of standard mixtures composed of weighed amounts of well-crystallized monoclinic and tetragonal/cubic phases. Well-crystallized tetragonal and cubic ZrO_2 standards were obtained from Magnesium Elecktron Ltd, Manchester. Well-crystallized monoclinic ZrO_2 was made by firing a dried ZrO_2 sol at 1600 °C for 4 h.

2.3. Electron microscopy

Electron microscopy was done with a Jeol 2000EX TEMSCAN operated at 200 kV with a LINK 10/85S EDS X-ray analyser. The LINK system offers a number of facilities, including quantitative X-ray analysis and element compositional mapping, as well as data processing.

Two techniques were used to prepare specimens for electron microscopy. One was to grind the samples in an agate mortar under acetone; the resulting powders were mounted on to a copper grid precoated with a thin holey carbon film. This method is useful when the crystalline particles are very small (< 0.1 μm), as occurs for poorly crystallized gel-precursor samples. Another method is to prepare a thin section for transmission electron microscopy by argon milling; this was used to observe grain boundaries in crystalline and more coherent matrices.

3. Results and discussion

3.1. X-ray diffraction

The XRD spectra of Al_2O_3–ZrO_2 gel (81.1% ZrO_2 + 18.9% Al_2O_3), ramped to progressively higher temperatures, are shown in Fig. 1. From room temperature to 200 °C, the gel remains nearly amorphous. It gives three very broad reflections centred at approximately 25.6°, 41.5°, 57.5° (2θ, CuK_α radiation). The first peak at 25.6° has a large shoulder at high 2θ angles. These reflections are considered to arise from the rudimentary structure of the gel. When the gel has been dried at 200 °C, it can be redispersed in water and, if the water : solid ratio is not too high, will reform a gel. The gel is not, however, clear. Probably the product contains some particulate matter. At 300 °C, the two X-ray diffraction peaks, at 41.5° and 57.5°, lose their separate identity. After heating at 300 °C, the solid will no longer reform a gel when rewetted. These changes indicate that a loss of gel structure occurs in the range 200–300 °C, accompanied by loss of structural water and anions, e.g. nitrate.

XRD spectra show that the glassy state persists upon continued heating to 800 °C, although some changes in XRD peak intensities occur. Crystalline ZrO_2 appears at 800 °C and initially the crystallite diffractions are very broad because the crystallites are small. Their nucleation must be inhomogeneous because X-rays show that amorphous material persists while crystallization is occurring (see also Section 3.4). The symmetry of the first-formed crystals is apparently cubic (c), thus preserving the cubic-like proto-structure of the gel. This similarity, supported by X-ray diffraction and high-resolution electron microscopy, has been widely used as an indicator of apparent c symmetry [28, 29]. Upon continued heating to 1000 °C, the crystalline component transforms to tetragonal (t) symmetry. Table I shows phase transformation and the crystal size changes, using the most intense X-ray reflection after treatment at different temperatures for 2 h.

The crystal size does not change uniformly; up to 1100 °C, it increases but between 1100 and 1200 °C, apparently decreases. This is because a new phase – monoclinic ZrO_2 (m) – nucleates and grows from ZrO_2 (t). At 800 and 900 °C, the crystal phase is ZrO_2 (c), but it transforms to ZrO_2 (t) at 1000 °C. The calculation of crystallite size based on Equation 1 is approximate, but its solutions give an order of magnitude indication of crystallite sizes: the results are comparable at least on a relative basis.

3.2. Phase transformation of ZrO_2 (t→m) with added CaO and MgO as stabilizers

The different polymorphs based on ZrO_2 may be stabilized to ambient by selectively incorporating other metal oxides, such as Y_2O_3, MgO and CaO [11, 12], with suitable conditions of heating and cooling. Upon addition of CaO. Table II shows (i) changes in X-ray d-spacing of the most intense X-ray reflection(s) for the polymorphs present; (ii) calculated crystallite sizes; (iii) phases present, and the content of the monoclinic phase. The starting gel composition is Zr : Al

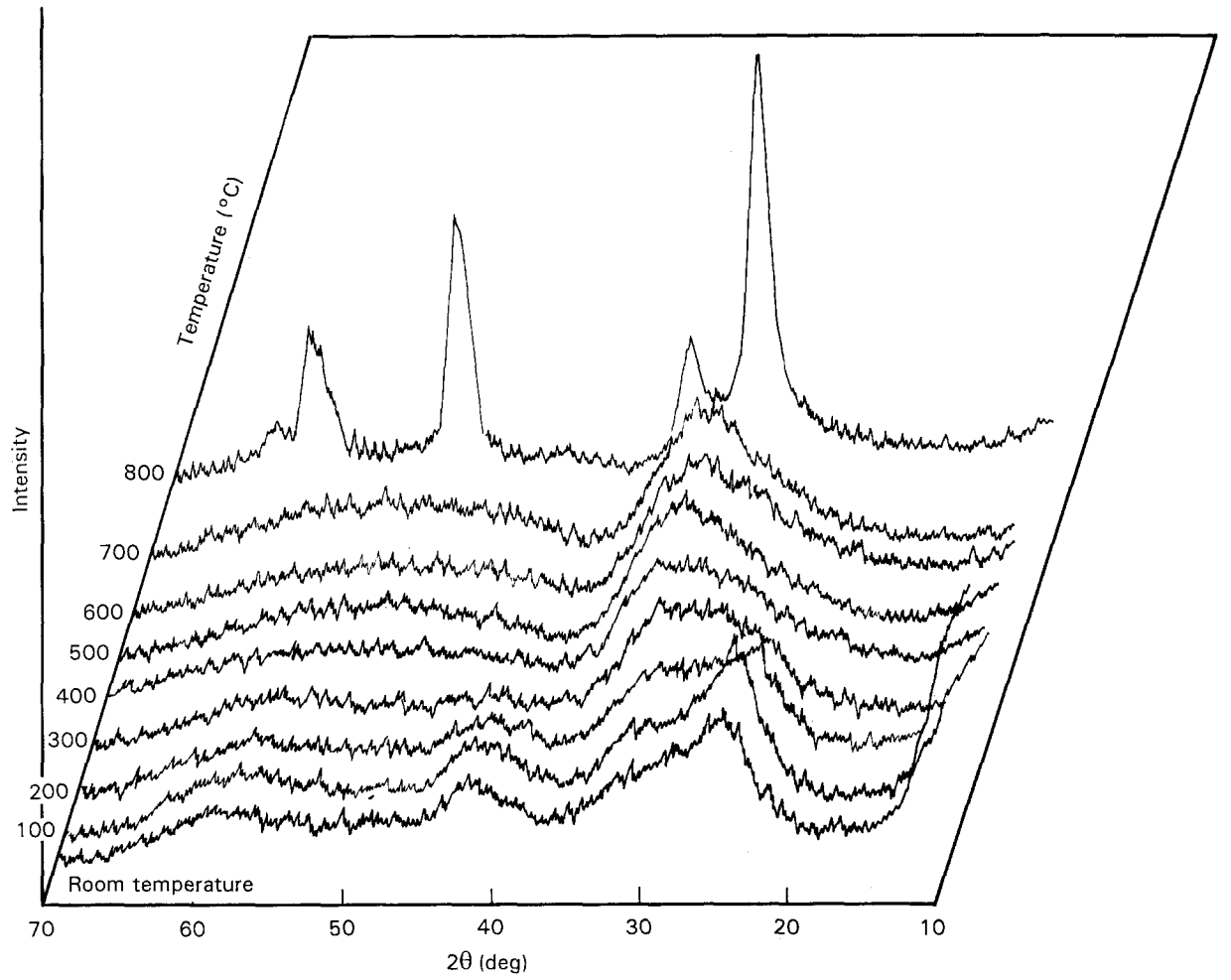

Figure 1 XRD spectra of ZrO_2–Al_2O_3 gel heated at different temperatures, gel composition: 18.9% Al_2O_3 + 81.1% ZrO_2 (by wt).

TABLE I Crystal size and calcination temperature: uniform 2 h calcination

	Temperature (°C)					
	800	900	1000	1100	1200	1300
Crystal size (nm)	28	31	49	81	70	115
Strongest reflection *d* (nm)	0.293	0.2936	0.2952	0.2962	0.3151	0.3170
Symmetry	(c)	(c)	(t)	(t)	(m)	(m)

Notes: (1) c = cubic, t = tetragonal, m = monoclinic.
(2) Gel composition: Zr:Al = 1.78:1 (molar ratio).

= 1.78:1 (molar ratio) and the Ca^{2+} precursor is $Ca(NO_3)_2$ solution (1.37 M in calcium). It also shows that crystallite size does not change uniformly, although it generally increases upon heating, except during the course of the phase transformation (t→m). The sequence of transformations upon heating is complicated by the effects of crystal size and chemical doping as well as phase transformations which may occur during cooling. The following account relates to heated samples, examined at ambient. The first-formed crystalline phase is still cubic, but transforms upon further heating to tetragonal at 1000 °C. After the monoclinic polymorphs begins to develop, the *d*-spacings of the remaining tetragonal polymorph decrease as the annealing temperature rises, eventually approaching the appropriate value for cubic. CaO can retard the transformation from tetragonal to monoclinic during heating; Fig. 2 shows phase changes in gels with different contents of CaO. The higher the content of CaO, the more tetragonal ZrO_2 persists through the thermal cycle. If no CaO is added, most of the ZrO_2 (t) transforms into ZrO_2 (m) between 1100 and 1200 °C. But as CaO is added, the transformation t→m occurs at progressively higher temperatures. However, most tetragonal ZrO_2 will have transformed to monoclinic ZrO_2 by 1450 °C using this heating programme: ramped at 15 °C min^{-1} from room temperature to the selected isotherm with a uniform dwell time of 2 h at each isothermal hold: Table II and Fig. 2. But more t phase can be obtained at 1600 °C if gels are first dried at 120 °C, then heated rapidly to 1600 °C; see Table III.

The content of ZrO_2 (t) is almost constant with time on any isotherm, but differs with temperature. In

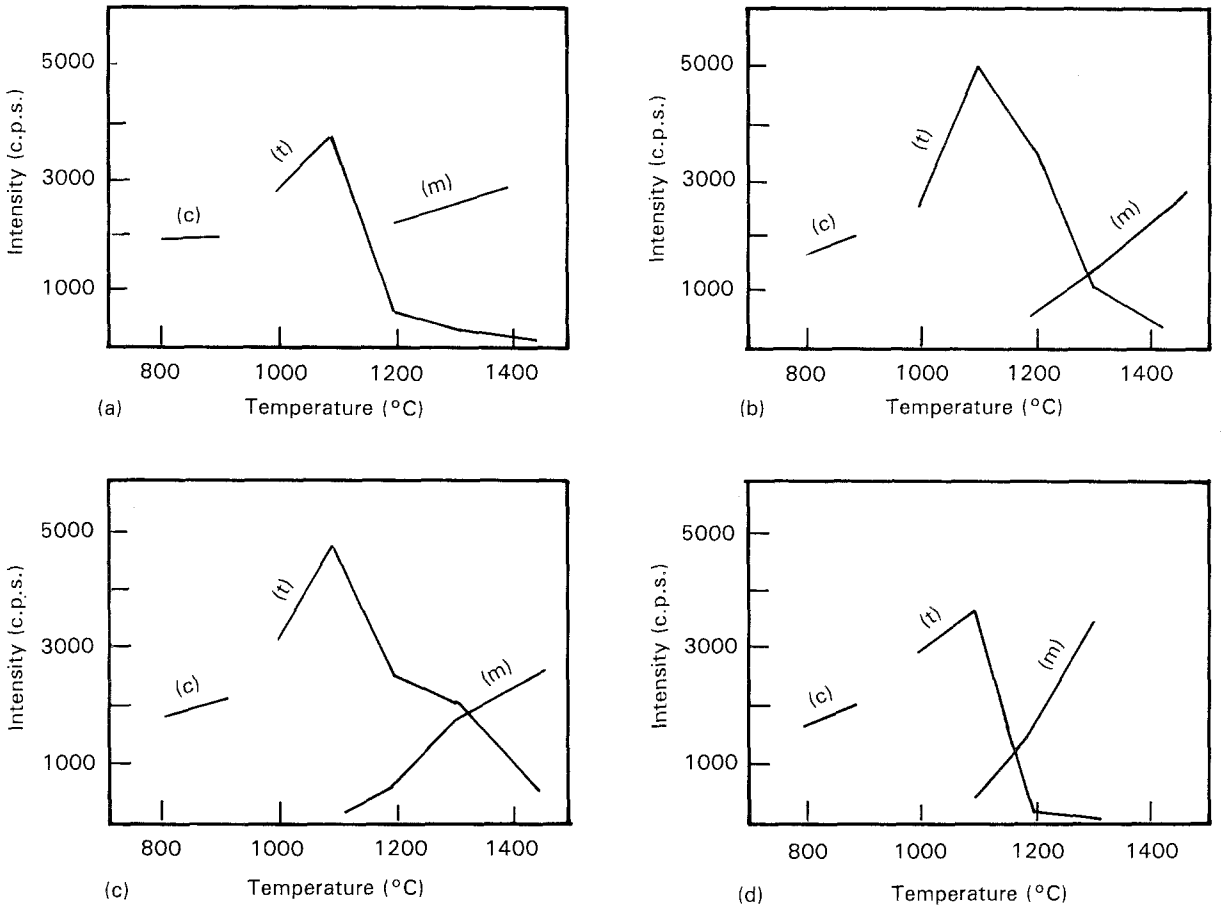

Figure 2 Phase transformation of the gels with different amounts of CaO addition. (a) 3.6%, (b) 5.3%, (c) 6.98%, (d) none.

TABLE II Selected properties of heated $CaO–ZrO_2$ gels

Sample		Temperature (°C)						
		800	900	1000	1100	1200	1300	1450
1. 0% CaO	Crystal size of main phase (nm)	28	31	48	80	69	118	
	m-ZrO_2 (wt%)	0	0	3.73	21.56	93.68	97.84	
	Symmetry	C	C	t	t, m	m, t	m, t	
	Most intense reflection nm	0.2930	0.2936	0.2952	0.2962, 0.3151	0.3151, 0.2945	0.3162, 0.2942	
2. 3.6 wt% CaO	Crystal size of main phase (nm)	27.5	29	48	85	70	75	105
	m-ZrO_2 (wt%)	0	0	0	11.32	84.56	92.06	96.50
	Symmetry	C	C	t	t	m, t	m, t	m, t
	Most intense reflection nm	0.2926	0.2932	0.2951	0.2957	0.3166, 0.2964	0.3168, 0.2950	0.3147, 0.2944
3. 5.3 wt% CaO	Crystal size of main phase (nm)	25	29	48	75	102	71	1.180
	m-ZrO_2 (wt%)	0	0	0	0	26.02	66.03	92.66
	Symmetry	C	C	t	t	t, m	m, t	m, t
	Most intense reflection nm	0.2933	0.2934	0.2959	0.2962	0.2961, 0.3157	0.3145, 0.2951	0.3148, 0.2941
4. 7.0 wt% CaO	Crystal size of main phase (nm)	24	29	48	98	98.5	62	102
	m-ZrO_2 (wt%)	0	0	0	2.69	19.98	53.45	80.59
	Symmetry	C	C	t	t, m	t, m	m, t	m, t
	Most intense reflection nm	0.293	0.2445	0.2954	0.2966, 0.3158	0.2961, 0.3156	0.3146, 0.2957	0.3148, 0.2947

TABLE III The content of ZrO_2 (t) as a function of time at 1600 °C (gel compostion: Zr:Al = 1.78:1, molar ratio)

	Time (h)					
CaO (wt%)	1.0	2.25	3.25	5.0	7.5	12
0.0	0[a]	0[a]	0[a]	0[a]	0[a]	0[a]
5.39	52.8	51.0	49.9	49.2	46.5	46.9
7.48	84.0	87.9	86.0	85.0	84.2	85.0
11.1	100	100	100	100	100	100

[a] All ZrO_2 is as the monoclinic polymorph.

Table II, for pure ZrO_2, most ZrO_2 is monoclinic (m) at 1450 °C for all compositions, but in the experiments recorded in Table III, with added CaO, m-ZrO_2 is only a minor phase. There appear to be two critical contents of CaO; a lower limit, below which no tetragonal phase develops and an upper limit, about 8% –9%, beyond which all tetragonal ZrO_2 is obtained.

Many data are available about the mechanism whereby metastable zirconia polymorphs are stabilized to room temperature by additives. Generally, it is thought that Zr^{4+} ions are replaced by lower-valent ion which leads to distortion of the structure and stabilizes normally-unstable polymorphs [30]. When CaO is the additive [31], O^{2-} vacancies are introduced to compensate for charge imbalance: the direction of the oxygen vacancies near Ca^{2+} is toward [3 3 2]. A displacement of O^{2-} ions in the [1 0 0] direction occurs, which makes it easy to form the t phase of ZrO_2. It is easy to speculate that this arrangement enhances the electrical conductivity.

It is interesting that ZrO_2 (c), not ZrO_2 (t), preferentially develops during sintering when MgO is included in the formulation; see Table IV.

As occurs with CaO as the stabilizer agent, there is a critical MgO content for partially stabilizing c-phase ZrO_2, between 4 and 6.7 wt% MgO. Below this, no cubic ZrO_2 phase exists. Above this limit, increasing MgO rapidly increases the content of cubic polymorph until by 13.4%, it is essentially all cubic.

In Mg-PSZ, the precipitates have a lenticular morphology with a (1 0 0) habit plane, and the critical particle diameter for phase transformation is ~0.2 μm [32]. In Ca-PSZ, the precipitates have an equiaxed morphology with a (1 0 1) habit plane and a critical particle size of ~0.1 μm [33].

3.3. Effect of Al_2O_3 on crystallization of ZrO_2

Crystallization depends strongly on the composition of the gel (Al/Zr ratio): the higher the Al/Zr ratio, the higher the temperature at which crystallization occurs. XRD spectra show that as the content of Al_2O_3 increases from 18.9 wt % (Fig. 1) to 81.1 wt % (Fig. 3), the crystallization temperature increases from 800 °C to 1000 °C. ZrO_2 is the first phase to nucleate and crystallize; Al_2O_3 needs a higher temperature to crystallize than ZrO_2. Thus, by XRD, the first weak gamma-alumina reflections appear around 1000 °C, but transformation to the stable polymorph (alpha-alumina) is only completed at 1200 °C.

TABLE IV The content of ZrO_2 (c) versus calcination time with different MgO contents at 1600 °C (gel composition: Zr:Al = 1.78:1, molar ratio)

	Time (h)			
MgO (wt%)	4.5	9.0	12.0	24
4.02	0[a]	0[a]	0[a]	0[a]
6.70	89.3	87.8	89.6	91.2
10.06	91.8	92.4	93.3	94.8
13.40	100	100	100	100

[a] All ZrO_2 is a monoclinic polymorph.

Table V shows data for the ZrO_2 polymorphs in two representative compositions. Both contain Al_2O_3 substantially in excess of the negligible amount which can be incorporated by solid solution in the crystalline structures of zirconia. Nevertheless, the effect of increasing the amount of free alumina is to increasingly stabilize the t-polymorph. For example, after ramping to 1300 °C the composition with 18.9% Al_2O_3 had little remaining tetragonal zirconia (2.2%) whereas in the higher alumina composition with 67.59% Al_2O_3, had 56% of the zirconia as the t-polymorph. The mechanism whereby a physical excess of Al_2O_3 stabilizes the tetragonal polymorph of ZrO_2 is unclear: it is suggested that it acts as a grain growth inhibitor for zirconia [5–7]. The unique microstructure developed from gel precursors, shown in subsequent figures, persists even upon prolonged sintering in air at 1600 °C; powder X-ray diffraction patterns exhibit line-broadened profiles for the ZrO_2 reflections and the grain size, as determined by electron microscopy, remains near the practical lower limits of resolution. Thus particle size, rather than aluminium in solid solution, is believed to be primarily responsible for stabilizing the t-polymorph.

3.4. Microstructural evolution of the gel during heating

Gels were ramped from room temperature to selected isotherms with a uniform dwell time of 2 h at each isotherm and were observed after each dwell stage by TEM. Depending on the extent to which sintering occurred, specimens were made by argon thinning (thin section, TSS); or powders (PS) for incoherent materials. The composition of the gel used for microstructural studies was: Zr:Al = 1.78:1 (molar ratio).

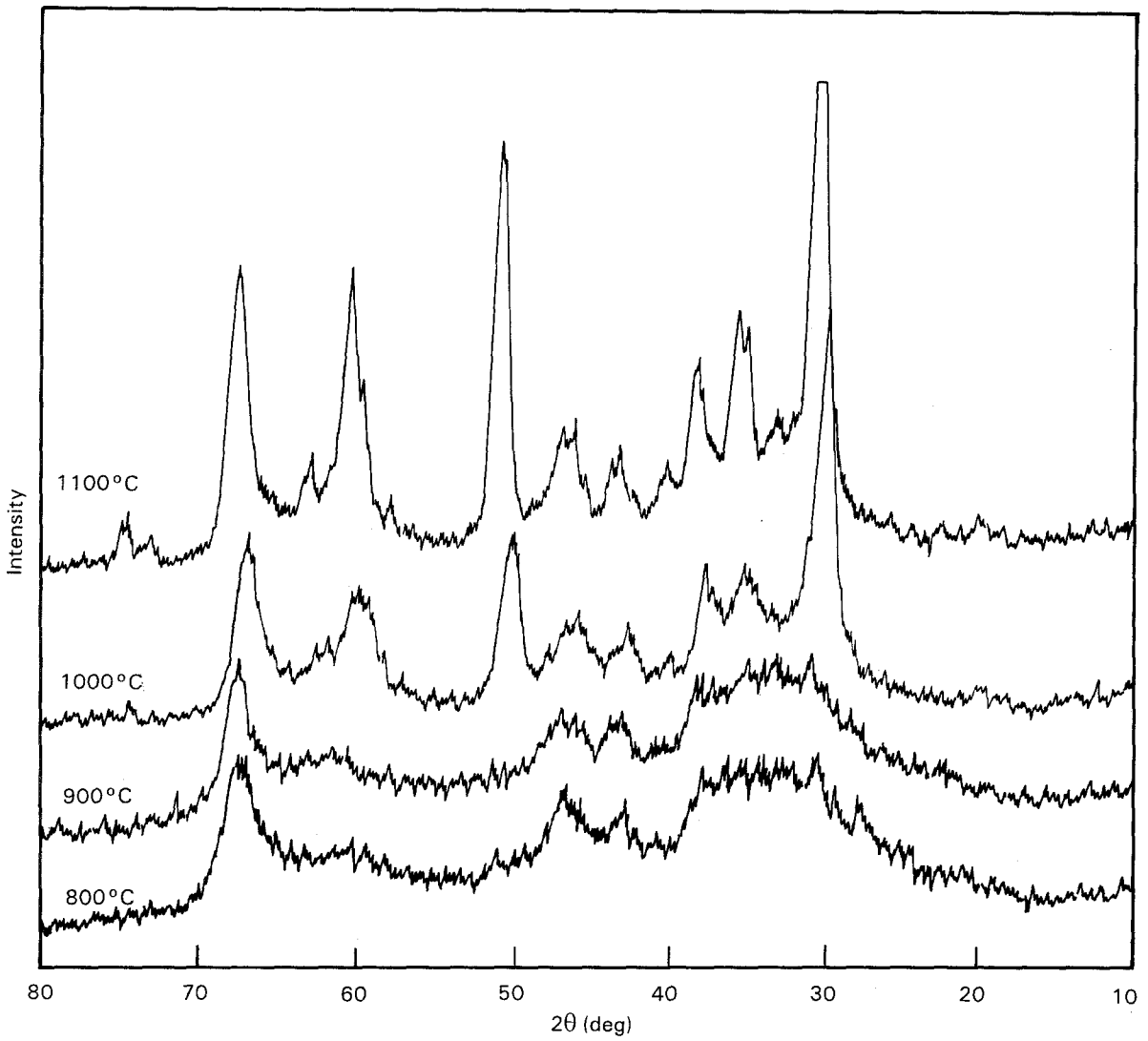

Figure 3 XRD spectra of Al_2O_3–ZrO_2 gel heated at different temperatures, gel composition: 82% Al_2O_3 + 18% ZrO_2 (by wt).

TABLE V The content of ZrO_2 (t) versus temperature as a function of composition

Gel composition	Temperature (°C)						
(wt%)	1000	1100	1200	1300	1400	1500	1600
ZrO_2 81.10% Al_2O_3 18.9%	96.3	74.9	6.3	2.2	0	0	0
ZrO_2 32.41% Al_2O_3 67.59%	100	100	59.5	56.4	49.2	38.1	38.2

According to XRD results, Fig. 1, the gel is essentially amorphous at low temperature. Transmission electron micrographs show that the gel still appears dense and homogeneous at 300 °C, see Fig. 4. Individual gel particles are too small to be resolved even at the maximum magnification of 500 000. The rudimentary grain structure of the gel in Fig. 4 is comparable with that of carbon film (seen at the top of the micrograph) and is thus characteristic of an amorphous material. It is concluded that the gel is homogeneous on a scale comparable with the point resolution of the microscope, 0.35 nm. So the gel must be ultrahomogeneous to a near-molecular scale. The gel continues to appear homogeneous with no component separation until crystallization occurs. At 400 °C, the TEM images are almost the same as at 300 °C, but the good densification is partially destroyed by mass loss accompanying thermal decomposition. There are some surface features, but no distinct internal morphological features. Upon heating to 500 and 600 °C, the gel develops a somewhat more granular structure but the phase boundaries remain indistinct. The size of the granular regions is still very limited and densification is poor. At 700 °C, more grain-like character appears; the grains are all below 10 nm and have diffuse borders with no crystalline character. In the range 300–700 °C, the electron diffraction patterns do not change and indicate the amorphous nature of the heated product.

At 800 °C, the gel structure appears quite open; the particle shape is typically vermicular, with particle sizes around 10 nm; see Fig. 5. The gel starts to

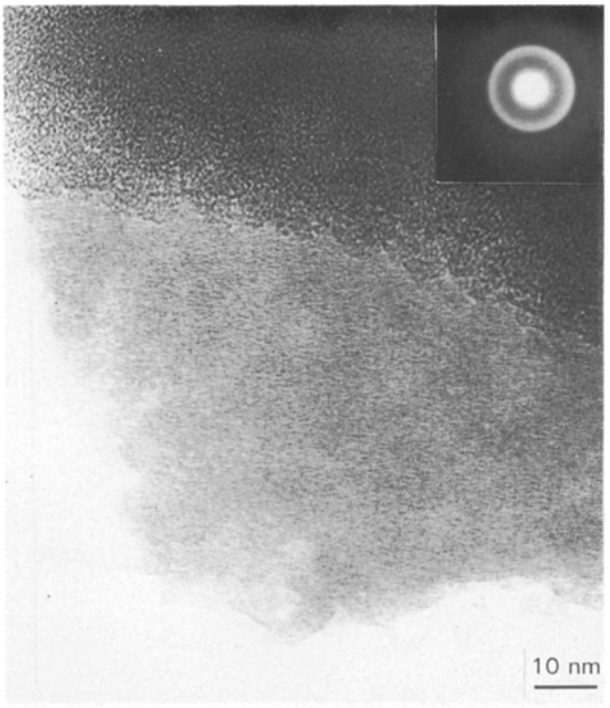

Figure 4 Micrographs of ZrO_2–Al_2O_3 gel (PS) heated at 300 °C.

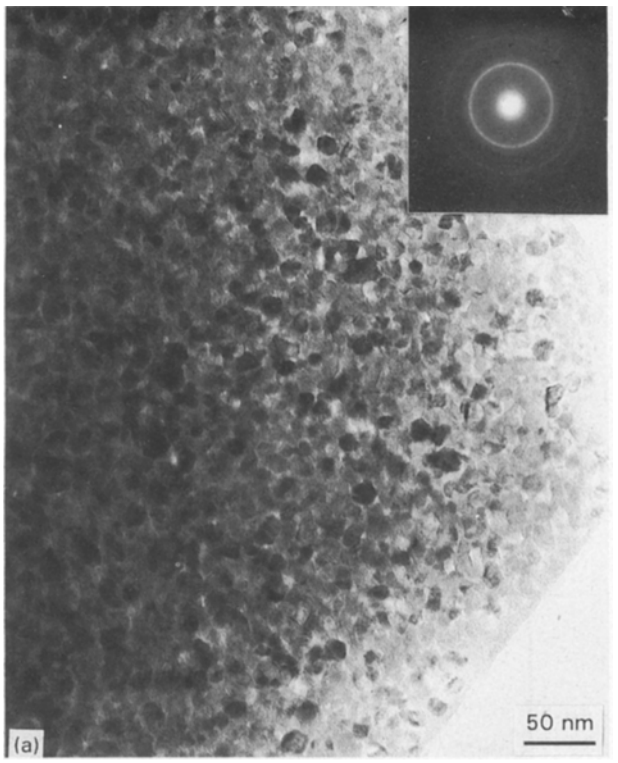

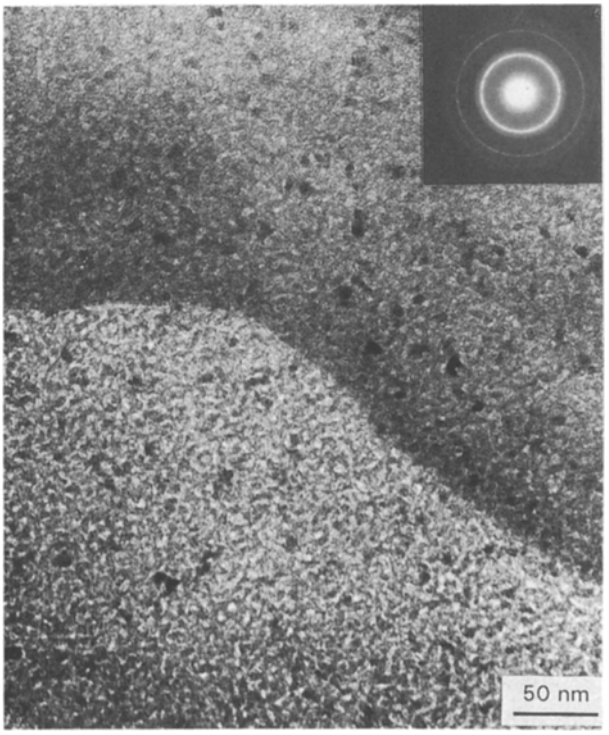

Figure 5 Micrographs of ZrO_2–Al_2O_3 gel (TSS) heated at 800 °C.

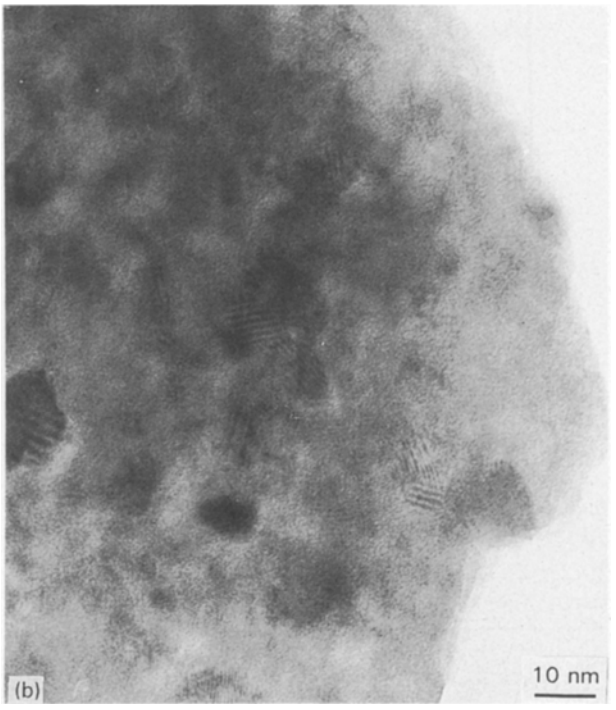

Figure 6 Micrographs of ZrO_2–Al_2O_3 gel heated at 1000 °C: (a) morphology of the gel (PS); (b) morphology of the gel (TSS).

crystallize at about this temperature. The optically dark grains are assigned to crystalline nucleii oriented with a major crystallographic zone parallel to the beam. Their nucleation must be inhomogeneous because the electron diffraction pattern shows a mixture of crystalline and amorphous components: most of the composition is probably still amorphous. At 900 °C, TEM clearly shows that the gel has a loose aggregation with irregular shapes; most of the particles are granular-like with sizes a little over 10 nm. Crystalline regions have begun to develop, but much amorphous material is still present.

At 1000 °C, particles of the order of 20 nm develop a more regular morphology; see Fig. 6a. Many lattice fringes and Moiré fringes begin to develop within the more crystalline regions; see Fig. 6b. An amorphous phase is still present and the boundaries between crystalline and amorphous regions remains indistinct. Crystalline particles (dark grains) are embedded in gel-like amorphous material or semi-crystalline alu-

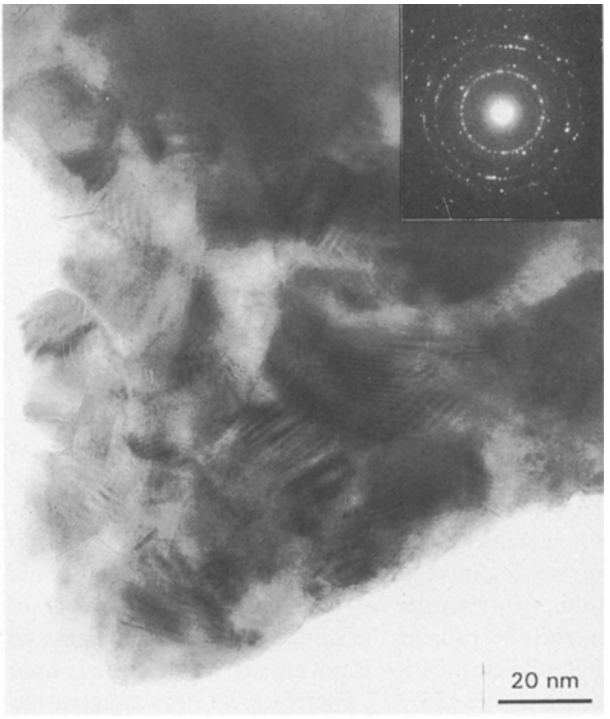

Figure 7 Micrographs of ZrO_2–Al_2O_3 gel (TSS) heated at 1100 °C.

mina. From these micrographs, very fine details can be seen: fine isolated and particle-like areas appear optically more dense in transmission than the lighter, more amorphous regions. The darker areas are assumed to correspond to the physically more dense regions and, because the powder is composed of only two components, alumina and zirconia, with different densities (3.67 g cm^{-3} for gamma alumina and 5.98 g cm^{-3} for tetragonal zirconia), the darker areas are probably ZrO_2. It is believed that the other phase is an amorphous gel, not crystalline alumina, because crystalline Al_2O_3 is not observed by X-ray diffraction until 1000 °C. During crystallization, homogeneity at the molecular scale will disappear gradually, because of component separation of ZrO_2 crystals in a still amorphous gel. This leads to subsequent continuing separation between crystalline ZrO_2 and Al_2O_3, as the latter crystallizes at higher temperatures. The higher the calcination temperature, the more important component separation becomes in defining the microstructure.

At 1100 °C, the particle size is still increasing, although most are below 50 nm. Very little amorphous phase remains and the size of regions showing lattice and Moiré fringes increases further; see Fig. 7. Energy

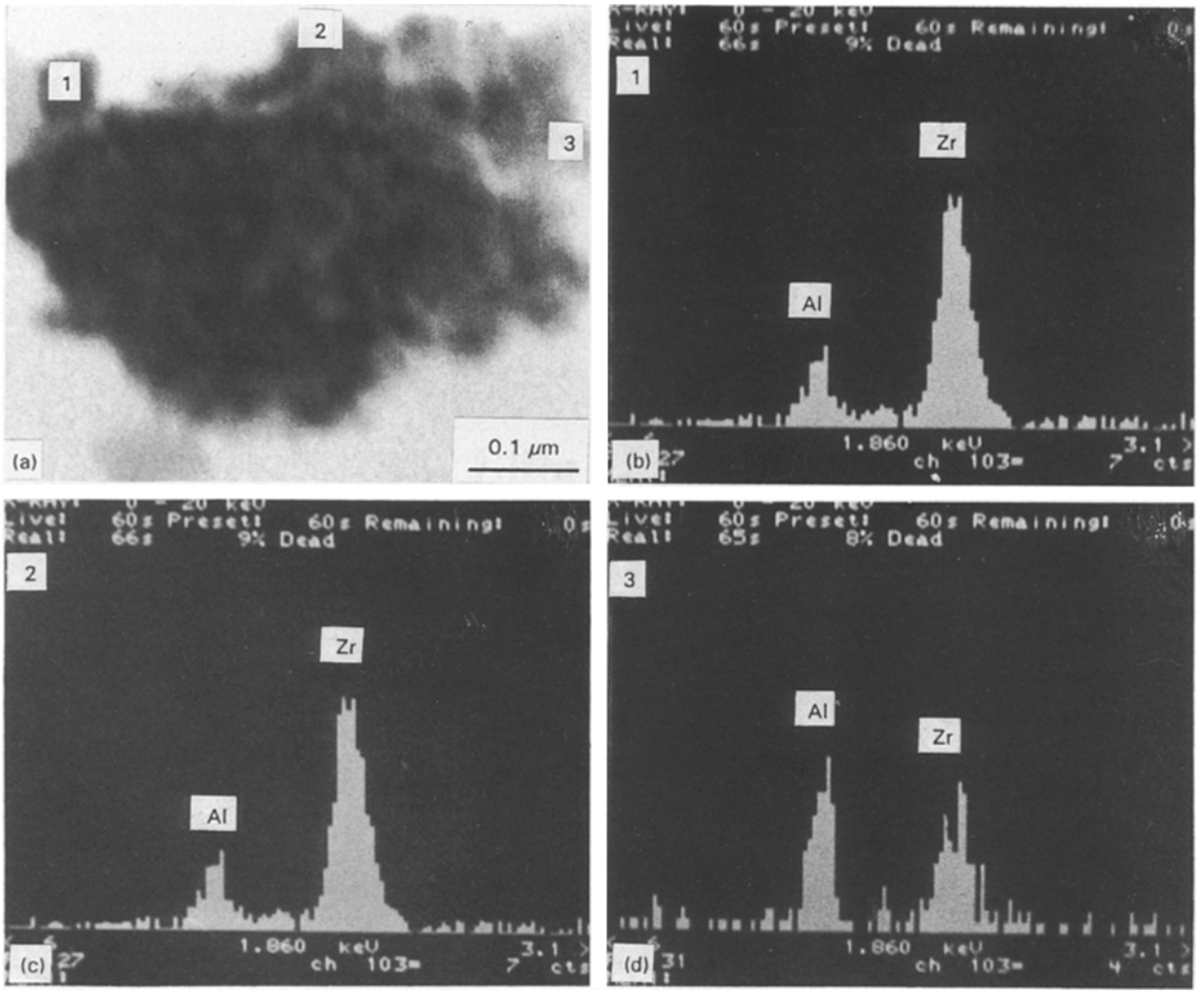

Figure 8 Electron-beam probe microanalysis of gel heated at 1100 °C: (a) original particles (PS); (b–d) energy dispersive spectroscopy of aluminium and zirconium in spots 1, 2, 3, respectively.

dispersive spectroscopy (EDS) of the gel shows that its chemical homogeneity in the range of electron-beam diameter starts to disappear at 1100 °C; see Fig. 8. Spots 1 and 2 show the gel is still homogeneous at electron-beam diameters (typically, a few tens of nanometers), but spot 3 is an alumina-rich area. The crystalline particle size at 1200 °C is about 100 nm, increasing to 200–500 nm at 1300 °C; see Fig. 9a. Calcination at higher temperatures causes progressively more component separation. Fig. 10 shows that the gel has lost homogeneity further at 1200 °C: spots 1 and 3 are alumina-rich areas; spot 1 has much more alumina than spot 3, while spot 2 is zirconia-rich. Figs 11 and 12 show the growth of a ceramic microstructure as the temperature increases: alumina starts to agglomerate from 1300 °C, until by 1450 °C it occurs mainly as well-defined aggregates.

Phase boundaries at 1300 °C become clear; see Fig. 9b. Some borders look mechanically well bonded and the boundaries are clear, while others remain indistinct. The distinct boundaries between ZrO_2 and Al_2O_3 appear to have a transition zone or interface, but this may be an artefact of the thinning process or because the grain boundaries are not perpendicular to the plane of the section. Certainly these interfaces have an important role in controlling the physical properties of ZrO_2–Al_2O_3 composites. The ZrO_2 crystals exhibit considerable internal structure which is believed to reflect their complex history of nucleation, growth and phase transformation.

Crystallization causes component separation and leads to loss of homogeneity. On other hand, crystallization reduces the rate of gel sintering. Densification of the gel during sintering is mainly achieved by viscous flow, which is orders of magnitude faster than diffusion-controlled processes which are typical in the sintering of crystalline materials [34, 35]. Therefore, the favourable course for densification is to sinter the gel to maximum densification before crystallization. As crystallization begins, the remaining gel would assist ceramic sintering because its viscous flow accommodates the progressive decrease in specific volume during sintering. But in these experiments, the gels were heated from 100 °C to high temperature in several steps with a 2.0 h hold at each intermediate temperature, not continuously. When crystallization begins, the gel densification is still incomplete, which may not be desirable: these factors are explored in more detail.

During isothermal holds at successively higher temperatures, water and anion portions are progressively lost; the resulting condensation reactions will increase the cross-link density; meanwhile, structural relaxation increases the skeletal density; these factors all lead to viscosity increases [36]. Thus, during an isothermal hold, the viscosity of a gel can rise by orders of magnitude, causing the sintering effectively to stop, so that full densification is not easy to reach at lower hold temperatures [35, 37]. Therefore, it is advantageous to continue heating during sintering, so that rising temperature compensates for structural relaxation and loss of OH^- and anions. This suggests that the faster the heating rate, the lower the temperature at which densification will be completed [35, 37]. However, excessively rapid heating will also cause trapping of evolved gases that can crack or bloat the gel.

The most important factors that can be used to control the degree of crystallization during sintering are composition, applied pressure, crystal impurities, and development of heterogeneous nuclei. Reducing the pore size speeds sintering without significantly affecting crystal nucleation or growth [38, 39]. The

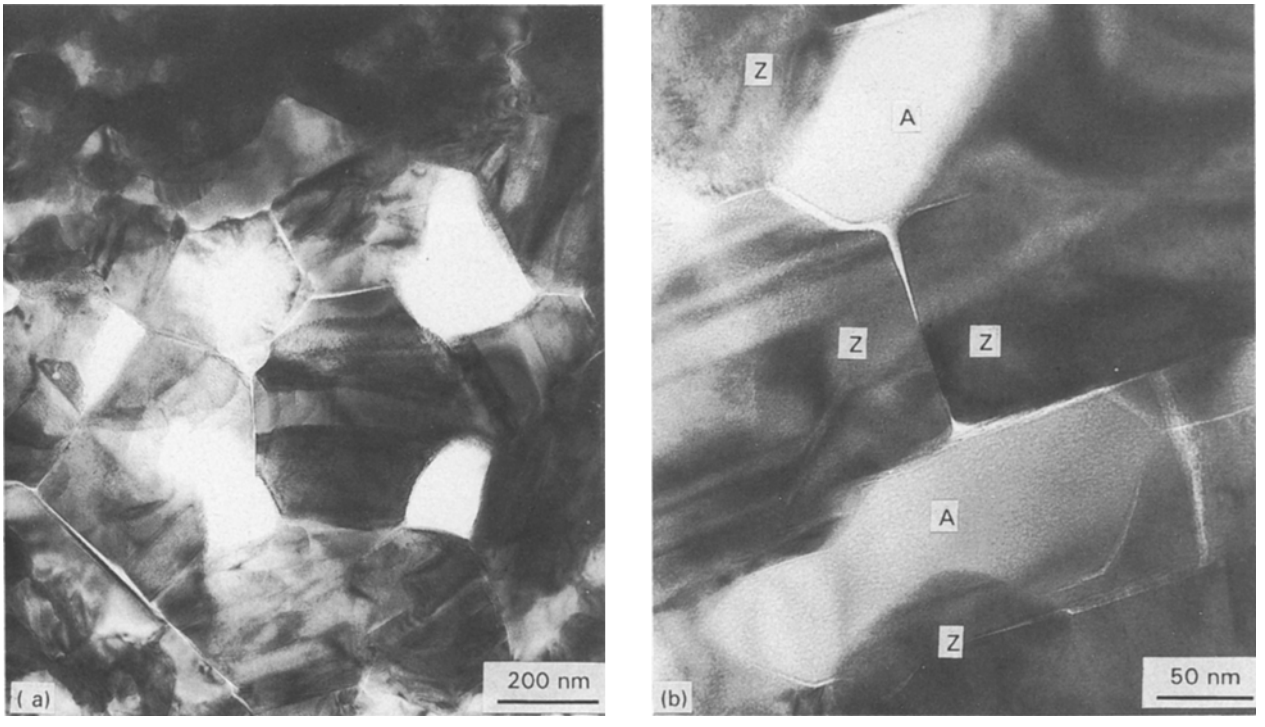

Figure 9 Micrographs of ZrO_2–Al_2O_3 gel (TSS) heated at 1300 °C: (a) morphology; (b) grain boundary: areas labelled A and Z are Al_2O_3 and ZrO_2, respectively.

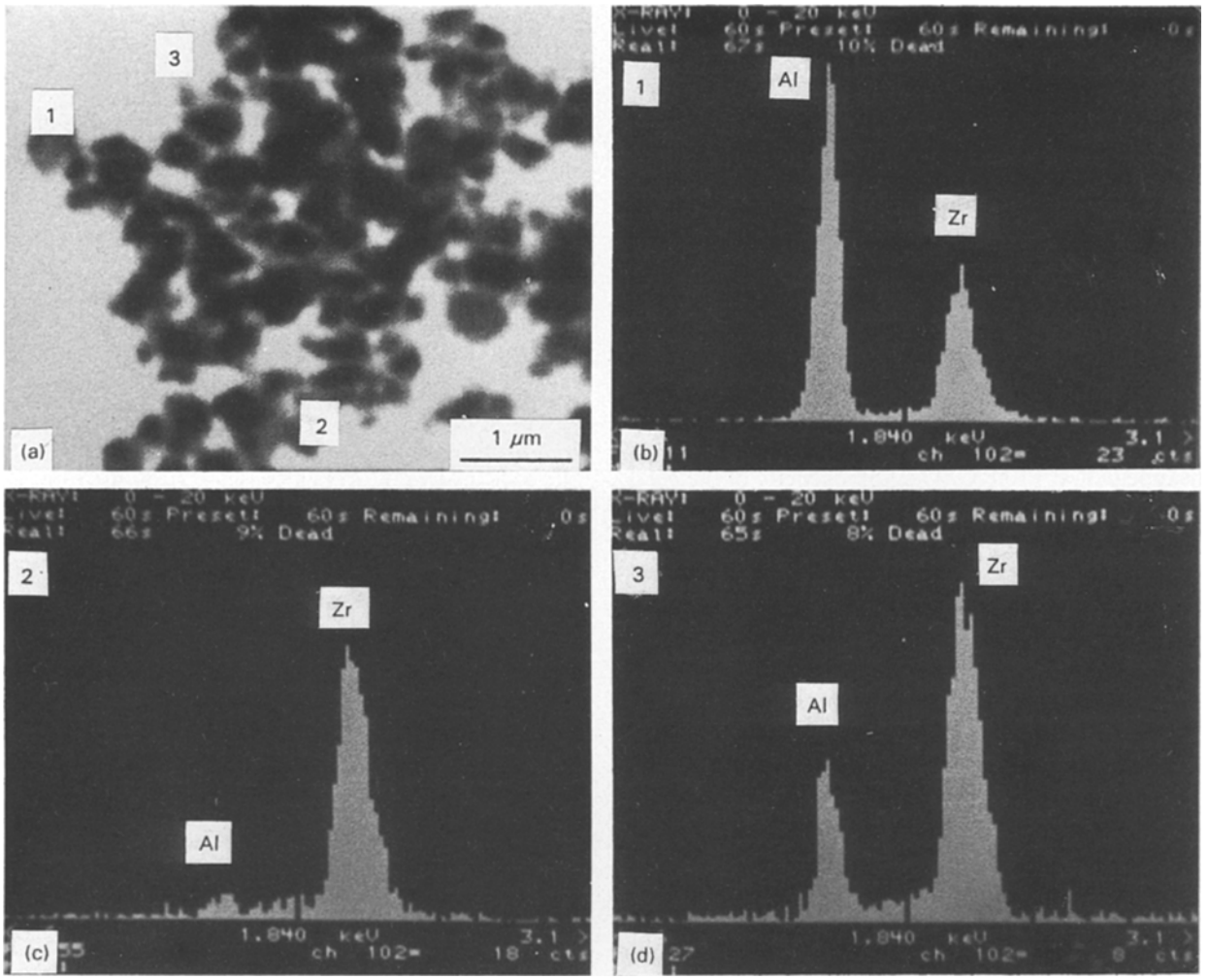

Figure 10 Electron-beam probe microanalysis of gel heated at 1200 °C: (a) original particles (Ps); (b–d) energy dispersive spectra of aluminium and zirconium in spots 1, 2, 3, respectively.

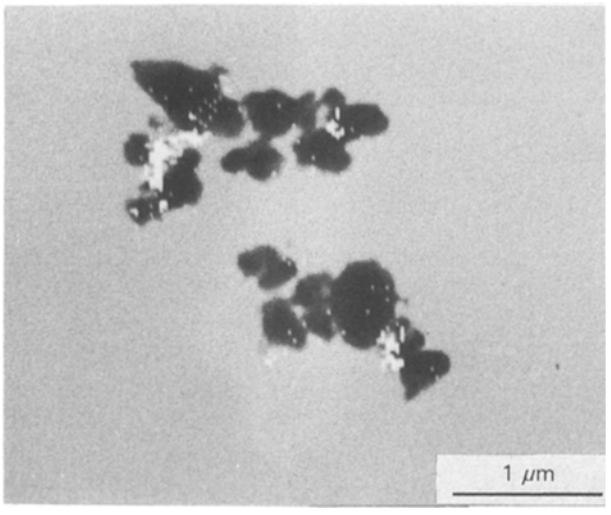

Figure 11 ZrO_2–Al_2O_3 gel at 1300 °C (PS), composite image made by superimposing digitized aluminium map (white) on STEM image to show Al_2O_3 concentrations.

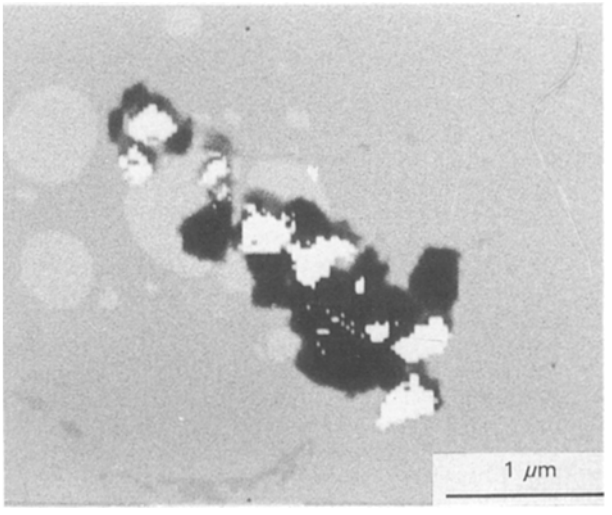

Figure 12 ZrO_2–Al_2O_3 gel at 1450 °C (PS), composite image made by superimposing digitized aluminium map (white) on STEM image to show Al_2O_3 concentrations.

sintering rate increases in proportion to the applied pressure, and in some systems, the effect of pressure on phase-transformation kinetics cannot be ignored. Heterogeneous nucleation reduces the thermodynamic barrier, rather than accelerating transport kinetics.

Gel densification with different heating programmes and gel physical properties, including shrinkage and flexural strength, are reported elsewhere and it is shown that good-quality ceramics can be obtained by sol–gel processing without the need to apply pressure during sintering [40].

4. Conclusions

Al_2O_3–ZrO_2 gel loses its H_2O and anion portions

gradually upon heating. At 300 °C, the structure of the gel is destroyed and the gel becomes nearly amorphous and glass-like. Crystallization occurs at 800 °C and the first-formed crystals are cubic ZrO_2, which gradually transforms to tetragonal ZrO_2. Metastable ZrO_2 phase assemblages, including cubic and tetragonal, can persist at ambient temperatures by incorporation of other metal oxides such as CaO and MgO. Al_2O_3 can also stabilize ZrO_2 (t) to ambient in sol–gel preparations. The heating programme has an important effect on the phase transformation.

Transmission electron micrographs reveal the development of the gel microstructure and crystallization. They also show that crystallization occurs at 800 °C. The amorphous materials have completely disappeared at 1100 °C. The homogeneity of the gel is gradually lost during firing, because of crystallization. At 1100 °C, it is almost homogeneous at the scale of a few tens of nanometres, but above 1200 °C, the microstructure coarsens. Al_2O_3 crystals begin to segregate and grow from 1300 °C.

Acknowledgement

The authors thank Banbury Laboratory, Alcan International Ltd, Oxon, UK, for financial support.

References

1. D. L. PORTER, A. G. EVANS and A. H. HEUER *Acta Metall.* **27** (1979) 1649.
2. N. CLAUSSEN, *J. Am. Ceram. Soc.* **59** (1976) 49.
3. T. K. GUPTA, J. H. BECHTOLD, R. C. KUZNIKI, L. H. CADOF and B. R. ROSSING, *J. Mater. Sci.* **12** (1977) 2421.
4. T. K. GUPTA, F. F. LANGE and J. H. BECHTOLD, *ibid.* **13** (1978) 1464.
5. Y. MURASE, E. KATO and K. DAIMON, *J. Am. Ceram. Soc.* **69** (1986) 83.
6. M. KAGAWA, M. KIKUCHI, Y. SYONO and T. NAGAE, *ibid.* **66** (1983) 751.
7. D. W. SPRONSON and G. L. MESSING, *ibid.* **67** (1984) C92.
8. B. J. J. ZELINSKI, C. J. BRINKER, D. C. CLARK and D. R. ULRICH (eds), "Better Ceramics Through Chemistry", MRS Symposia Proceedings, Vol. 180 (Materials Research Society, Pittsburgh, PA, 1990) p. 1099.
9. C. J. BRINKER, D. C. CLARK and D. R. ULRICH (eds), "Better Ceramics Through Chemistry", MRS Symposia Proceedings, Vol. 73 (Materials Research Society, Pittsburgh, PA, 1986) p. 822.
10. *Idem*, "Better Ceramics Through Chemistry", MRS Symposia Proceedings, Vol. 121 (Materials Research Society, Pittsburgh, PA, 1988) p. 900.
11. L. L. FEHRENBACHER and L. A. JACOBSON, in "Rare Earth Research III" edited by L. Eyring (Science Publishers, New York, 1965) p. 687.
12. J. G. DUH and M. Y. LEE, *J. Mater. Sci.* **24** (1989) 4467.
13. A. H. HEUER, *J. Am. Ceram. Soc.* **70** (1987) 689.
14. V. S. NAGARAJAN and K. J. RAO, *J. Mater. Sci.* **24** (1989) 2140.
15. A. H. HEUER, N. CLAUSSEN, W. M. KRIVEN and M. RUHLE, *J. Am. Ceram. Soc.* **65** (1982) 642.
16. M. YOSHIMURA, *Am. Ceram. Soc. Bull.* **67** (1988) 1950.
17. WENBANG ZHANG and F. P. GLASSER, *J. Eur. Ceram. Soc.* **11** (1993) 143.
18. WENBANG ZHANG and F. P. GLASSER, *J. Mater. Sci.* **28** (1993) 1129.
19. *Idem, J. Eur. Ceram. Soc.* **11** (1993) 149.
20. J. L. WOODHEAD, *J. Mater. Educ.* **6** (1984) 887.
21 W. E. GARNER, "Chemistry of the Solid State" (Butterworths Scientific, London 1955) pp. 109–12.
22. H. P. KLUG and L. E. ALEXANDER, "X-ray Diffraction Procedures for Polycrystalline and Amorphous Materials" (Wiley, New York, 1954) pp. 491–538.
23. R. GARVIE and P. NICHOLSON, *J. Am. Ceram. Soc.* **55** (1972) 303.
24. P. A. EVANS, R. STEVENS and J. G. P. BINNER, *Br. Ceram. Trans. J.* **83** (1984) 39.
25. R. H. HANNINK, *J. Mater. Sci.* **13** (1978) 2487.
26. R. A. MILLER, J. L. SMIALEK and R. G. GARLICK, in "Advances in Ceramics", Vol. 3, "Science and Technology of Zirconia", edited by A. H. Heuer and L. W. Hobbs (American Ceramic Society, Columbus, OH, 1981) pp. 241–53.
27. H. K. SCHMID, *J. Am. Ceram. Soc.* **70** (1987) 367.
28. J. R. FRYER, J. C. HUTCHISON and R. PATERSON, *J. Coll. Interface Sci.* **34** (1979) 238.
29. A. CLEARFIELD, *Rev. Pure Appl. Chem.* **14** (1964) 91.
30. H. O. SHIH-MING, *Mater. Sci. Eng.* **54** (1982) 23.
31. J. B. COHEN, J. FABOR Jr and M. MORINAGA, in "Advances in Ceramics", Vol. 3, edited by A. H. Heuer and L. W. Hobbs, (American Ceramic Society, Columbus, OH, 1981) p. 37.
32. D. L. PORTER and A. H. HEUER, *J. Am. Ceram. Soc.* **60** (1977) 183.
33. R. H. J. HANNINK, K. A. JOHNSTON, R. T. PASCOE and R. C. GARVIE, in "Advances in Ceramics", Vol. 3, "Science and Technology of Zirconia", edited by A. H. Heuer and L. W. Hobbs (American Ceramic Society, Columbus, OH, 1981) pp. 116–36.
34. R. W. HOPPER and D. R. UHLMANN *Mater Sci. Eng.* **15** (1974) 137.
35. G. W. SCHERER, in "Sol–Gel Science and Technology, Proceedings of the Winter School on Glasses and Ceramics from Gels", edited by M. A. Aegerter, M. Jafelicci Jr, D. F. Souza and E. D. Zanotto, Sao Carlos (SP), Brazil, August 1989, World Scientific Publications, Singapore, pp. 221–256.
36. T. A. GALLO and L. C. KLEIN, in "Better Ceramics Through Chemistry II", Materials Research Society Symposia Proceedings, Vol. 73, edited by C. J. Brinker, D. E. Clark and D. R. Ulich (North-Holland, New York, 1986) pp. 245–50.
37. C. J. BRINKER and G. W. SCHERER, "Sol–Gel Science: The Physics and Chemistry of Sol–Gel Processing" (Academic Press, San Diego, CA, 1990) pp. 675–744.
38. J. ZARZYCKI, in "Advances in Ceramics", Vol. 4 (American Ceramic Society, Columbus, OH, 1982) pp. 204–16.
39. *Idem, J. Non-Cryst. Solids.* **48** (1982) 105.
40. WENBANG ZHANG and F. P. GLASSER, *J. Eur. Ceram. Soc.*, in press (1993).

Received 15 March
and accepted 7 May 1993